

# Parity Violation in High-Energy Electron Scattering: Data Analysis for the $G^0$ Experiment

A thesis submitted in partial fulfillment of the requirement of the  
degree of Bachelor of Science with Honors in Physics  
from the College of William and Mary in Virginia,

by

Aimee C.E. Slaughter

Accepted for \_\_\_\_\_

\_\_\_\_\_  
Advisor: Prof. David Armstrong

\_\_\_\_\_  
Prof. Todd Averett

\_\_\_\_\_  
Prof. Henry Krakauer

\_\_\_\_\_  
Prof. Nahum Zobin

Williamsburg, Virginia  
May 2004

## Abstract

The focus of the  $G^0$  experiment at Jefferson Lab is the contribution of the strange quark to the character of the proton. The effects of different flavors of quarks can be disentangled by comparing the electromagnetic and weak contributions, since the electromagnetic and weak couplings of the various flavors differ. The weak interaction can be isolated for study because it violates parity symmetry, so there is a difference in the scattering rates of electrons with their spins aligned with their momentum and those with oppositely aligned spins. The electron beam being collided with the proton target, however, carries with it a halo: a non-Gaussian fringe caused by interactions with stray gas in the beam enclosure, the beamline, the beam itself, etc. The halo could adversely affect the results of the experiment, especially if it is helicity-correlated, since  $G^0$  is a parity violation experiment. It is therefore important to characterize the beam halo, which is monitored with a halo target (of two possible sizes) and several halo monitors. The halo monitors themselves are characterized to investigate the extent of their reliability and applicability. After establishing this, the halo rates are analyzed in several ways to determine what sort of beam halo the experiment usually has to contend with. Overall, it seems that the halo monitors perform as expected, and that the halo is within reasonable bounds. Having the halo monitors and target in place during experimental runs provides valuable insight into the quality of the beam.

## 0.1 Introduction

There is a fundamental human curiosity about how things work and what things are made of. We have found that all matter is comprised of atoms, and atoms themselves of protons, neutrons, and electrons (protons and neutrons are collectively referred to as nucleons, since they create the nucleus). Now it is apparent protons and neutrons also have a substructure: a trio of quarks. The proton, for example, has a primary structure of two up quarks and a down quark. Quarks come in six flavors: up, down, strange, charm, top, and bottom. Each flavor has distinctive properties.

Quarks stay bound together in a nucleon by exchanging gluons, the carriers of the strong force. The uncertainty principle allows for the creation of virtual particle-antiparticle pairs during such exchanges, so along with the one down and two up quarks in the proton, there is also a sea of virtual quark-antiquark pairs. The lifetime for a quark-antiquark pair is inversely related to the mass of the quark, so the strange quark, which is the third lightest flavor after up and down quarks, is expected to have the greatest effect in the proton's virtual sea.

The influences of this sea on the properties of the proton or neutron are quite interesting and not yet suitably explained by theory. Experimental guidance is needed, and thus the  $G^0$  Experiment[1] at the Thomas Jefferson National Accelerator Facility (JLab) was undertaken. By colliding a beam of polarized electrons with a proton target,  $G^0$  aims to uncover many of the effects of the strange quark on the proton sea. The interactions between the beam and target are governed by both electromagnetic and neutral weak forces. The electromagnetic and weak couplings of each quark are different, and so the effects of each flavor can be disentangled from each other. The weak interaction can be isolated for study because it violates parity symmetry: there is a difference in the scattering rates of electrons with their spins aligned with their momentum and those with oppositely aligned spins. For confidence in the results, however, we must understand the character of the electron

beam. The beam may carry a halo – a non-Gaussian tail of extraneous electrons around the beam itself – which would interfere, perhaps significantly, with the data if not corrected for.

## 0.2 Physics Background

The data from  $G^0$  will hopefully illuminate properties of nucleons, and the effects of their quark seas, as yet unknown. Understanding some of the theory about quarks is therefore useful (for a more detailed discussion of this, see [2]). Just as quantum electrodynamics (QED) describes the exchange of photons between charges, quantum chromodynamics (QCD) describes the exchange of gluons between quarks. From the Standard Model we know that photons are the force carrier particle for the electromagnetic force and that gluons carry the strong force; photons, however, carry no charge while gluons carry both a color and an anticolor (that do not result in net colorlessness). QCD is like QED in that opposite colors attract and like colors repel. It can also be shown that anti-symmetrical quantum states cause different colors to attract and symmetrical quantum states cause different colors to repel. Interestingly, QCD does not require the existence free quarks to be forbidden. It actually allows for asymptotically free quarks in the limit of high  $Q^2$ , where  $Q^2$  is the momentum transfer.

Experimentally, it has been found that the effect of antiup and strange quarks to the longitudinal momentum of protons and neutrons (collectively named nucleons) is of the same order (several percent) of antiup and antidown quarks' effect.[3] The contribution of strange quarks to nucleon charge and magnetism can be found using existing measurements of nucleon electromagnetic form factors and parity-violating electron scattering experiments such as  $G^0$ . Parity violation is essential here, because that is the key to disentangling the effects of the different quark flavors. The photons' coupling to quarks is proportional to the electric charge of the quarks; similarly, the  $Z^0$ 's coupling

is directly related to the weak charge of the quarks. The interference of electromagnetic and weak currents violates parity because the weak interaction violates parity, thus measurements sensitive to  $\gamma$  and  $Z^0$  exchange allow the different quark flavors to be isolated.

### 0.2.1 Theory

Letting  $f = \text{flavors}$ , the elementary quark currents in the nucleon are:

$$J_\mu^i = \langle N | \sum_f e_f^i \bar{q}_f \Gamma_\mu q_f | N \rangle \quad (1)$$

where  $i$  encodes electromagnetic or neutral weak currents, and  $\Gamma_\mu$  is  $\gamma_\mu$  for vector currents and  $\gamma_\mu \gamma_5$  for the weak axial current.[4] The axial current  $G_A$  and form factors  $G_{E,M}^\gamma$  and  $G_{E,M}^Z$  are of interest to us, and can be defined in the following way[4]:

$$G_A = G_A^U - (G_A^d + G_A^s) \quad (2)$$

$$G_{E,M}^\gamma = \frac{2}{3} G_{E,M}^U - \frac{1}{3} (G_{E,M}^d + G_{E,M}^s) \quad (3)$$

$$G_{E,M}^Z = (1 - \frac{8}{3} \sin^2 \theta_W) G_{E,M}^U + (-1 + \frac{4}{3} \sin^2 \theta_W) (G_{E,M}^d + G_{E,M}^s) \quad (4)$$

Assuming charge symmetry, these equations, which hold true for the proton, can be expressed for the neutron by exchanging  $u$  for  $d$ ,  $\bar{u}$  for  $\bar{d}$ , and vice versa. Charge symmetry is an important assumption here[5]: if this symmetry holds, nucleons only differ under the exchange of up and down quarks.  $G_E$  and  $G_M$  are essentially Fourier transforms of the charge and current distributions.

An experimental asymmetry arises because of the parity violation. Denoting the cross-sections from right- and left-handed electrons by  $\sigma_R$  and  $\sigma_L$ , the asymmetry can be expressed as

$$A = \frac{\sigma_R - \sigma_L}{\sigma_R + \sigma_L}. \quad (5)$$

### 0.2.2 JLab Overview

The experiment suggested by the above theory requires a rather involved setup: namely, a particle accelerator. At JLab there is an electron beam available to three experimental halls simultaneously. The beam is created at the injector, by polarized laser light incident on strained-layer GaAs wafers in a 100 kV electron gun. The crystal being strained is useful because the  $\frac{3}{2}$  energy states have been forced out of having the same energy, so the laser can be tuned to a frequency that targets the  $\pm\frac{3}{2}$  states that can then promote an electron to either of the two  $\frac{1}{2}$  energy states. The GaAs photo-cathodes are exposed to atomic hydrogen to clean the surface and then the activation energy of the surface is reduced by introducing Ce and then nitrogen trifluoride. There are three separate laser systems, one for each hall; and each has an optical pulse train locked to the accelerator's radio frequency. For  $G^0$ , a Ti:Sap laser is required, rather than the regular diode laser, to achieve an electron beam repetition rate of 31.1875 MHz and average current of  $40\mu\text{A}$ . [6]

The electron beam leaves the injector, and enters the ring. The ring is ovoid and comprised of two linear accelerators connected by two half-turns. The linacs accelerate the electrons in bursts by channelling them through potential differences. Series of quadrupole magnets focus the beam. Each quadrupole magnet focuses the beam along one axis. The electrons make up to five circuits before being diverted into one of the three experimental halls.

### 0.2.3 $G^0$ Experiment

$G^0$  is underway in Experimental Hall C. It derives its name from  $G_E^0$  and  $G_M^0$ , the elastic flavor singlet form factors being measured.  $G_E^0$  is the charge form factor, and  $G_M^0$  the magnetic.  $G^0$  is

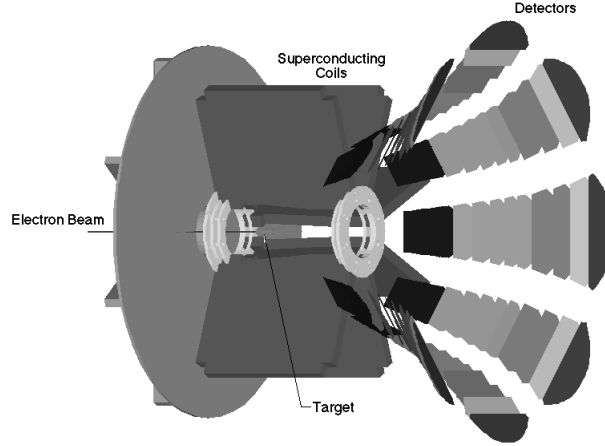


Figure 1:  $G^0$  Spectrometer

taking the first direct measurements of the quark-antiquark sea in low energy observables.[7]

Shown in *Figure 1* is the toroidal superconducting spectrometer being used in  $G^0$ . Particles of the same momentum and scattering angle are focused onto the detectors by a magnetic field. The detectors are arranged in octants around the “Ferris Wheel;” four of the octants are the responsibility of the North American part of the collaboration, and four are of the French. Each octant has 16 pairs of scintillators, each pair defining a layer of the detector[8]. To investigate the parity violation central to the experiment, the electron beam is flipped at 30 Hz between the two helicity states—that is, with the electrons’ momentum aligned and anti-aligned with their spin.

$G^0$  has a broad  $Q^2$  range, between .12 and 1.0  $\text{GeV}^2$  in the forward orientation and at .25, .5, and .8  $\text{GeV}^2$  in the backward orientation. The electron beam runs at 3.0 GeV and 40  $\mu\text{A}$ , colliding with a 20 cm liquid H target. There are forward and backward orientations of the detecting equipment: the forward set-up measures at small angles where  $G_E^0$  dominates, and the backward set-up measures at larger angles where  $G_M^0$  is dominant. Protons will be separated from pions in the forward configuration using time-of-flight measurements; in the backward configuration Cerenkov counters

and another scintillator array will be needed.

#### 0.2.4 Beam Halo

It is not empirically obvious whether the beam halo could be correlated with the helicity of the electron beam. If it were, a false asymmetry would very easily be created. The formation of beam halo in a high-energy electron accelerator is not well understood, but probable causes include the electron beam scraping the beam pipe, scattering against stray gas in the beam line enclosure, or self-interacting. Halo might also arise from refracted or scattered laser light hitting the photocathode surface in the electron source[9]. Monitoring and characterizing the beam halo ensures that it stays within the experiment's specifications and also allows it to be actively minimized (by adjusting beam steering, etc.).

Halo can interfere in several ways with the data from the experiment: it increases the "singles" rates in the detectors (non-coincident events that are likely due to background) and the general background radiation, lowering the lifetime of the photomultiplier tubes (PMTs) and increasing the dead time in the detectors. The halo could also interact with the target cell walls, which would increase the number of inelastic protons measured; the subtraction of the effect of the inelastic protons under the elastic proton peak is a major contribution to the uncertainty in the  $G^0$  experiment. The halo could also possibly be helicity-correlated, which could then create a false asymmetry, since  $G^0$  is a parity-violation experiment. The requested limit for the halo on the  $G^0$  experiment is 1 part per million (ppm) outside a 6 mm radius. By better understanding the beam halo, verifying whether it's within the specified limit and investigating possible helicity correlation, the uncertainty on the final results of the experiment can be reduced.

To measure the halo both continuously and in specific checks, a sort of "anti-target" is used. The halo targets are holes of specific size through which the beam passes, hopefully centered with



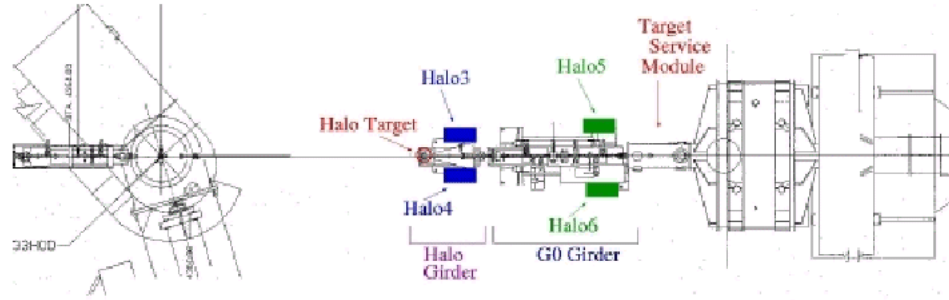


Figure 2: Positions of the Halo Target and Halo Monitors 3-6 Along the Beampipe (overhead view)

the center of the circular hole. The beam (if steered correctly) should pass unaffected through the target hole, while the halo surrounding the beam scrapes against the target sides and creates a shower of particles we can then detect. The two targets are mounted on an apparatus that allows smooth transitions in and out of the beam, and are of 2 mm-thick carbon, one with a radius of 6 mm for specific checks and one of 11 mm radius for continuous monitoring. The smaller-radius target is used primarily for spot checks since it is right on the edge of the requested halo limit. The 11 mm target gives the beam some leeway for slightly errant steering or halo, but is small enough to be a very useful check on the size of the halo. Either one of the targets or neither of them can be present in the beam, depending on what sort of run is being taken. There is an array of six detectors downstream from the target; their positions are shown in *Figures 2* and *3*.

The halo monitors are photomultiplier tubes (PMTs) attached to scintillators. An incoming particle interacts with the piece of scintillating material in such a way to create a photon, which can then strike the PMT face. Travelling through the glass face, the photon hits the photocathode, and an electron is created as described by the photoelectric effect. There are then a series of dynodes which attract and accelerate the photon; at each dynode more electrons are created until the last dynode is reached and there are enough electrons to form an electronic signal which can be processed.

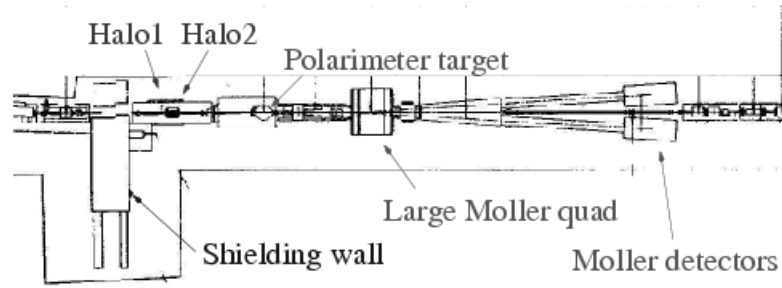


Figure 3: Positions of Halo Monitors 1 and 2 in the Beam Alcove Upstream of Hall C (overhead view)

Therefore, despite their name, PMTs do not create photons but electrons: what they multiply is the signal from one photon striking the PMT.

### 0.3 Methods

Sarah Phillips and I installed two halo detectors, Halos 3 and 4, in Hall C. Each detector is a PMT coupled via a silicone cookie with a small piece of Lucite; the whole detector is ensconced in Tedlar and black electrical tape to ensure that it is light-tight. We worked to characterize the detectors before we put them in place in the hall. Plots characterizing both detectors are shown in *Figures 4* and *5* – in these measurements the signals from the detectors have been fed through a discriminator before being sent to the oscilloscope as the trigger, with the undiscriminated signal being displayed. These signals demonstrate healthy PMTs. The rise time is quick (around 3 nanoseconds). There are more shallow curves than deep ones: the shallowest ones represent single photoelectron events, while the deeper ones probably result from cosmic rays.

The positions of Halo 3 and 4 along the beam line are shown in *Figure 6*. We mounted them on aluminum ledges on either side of the halo girder.

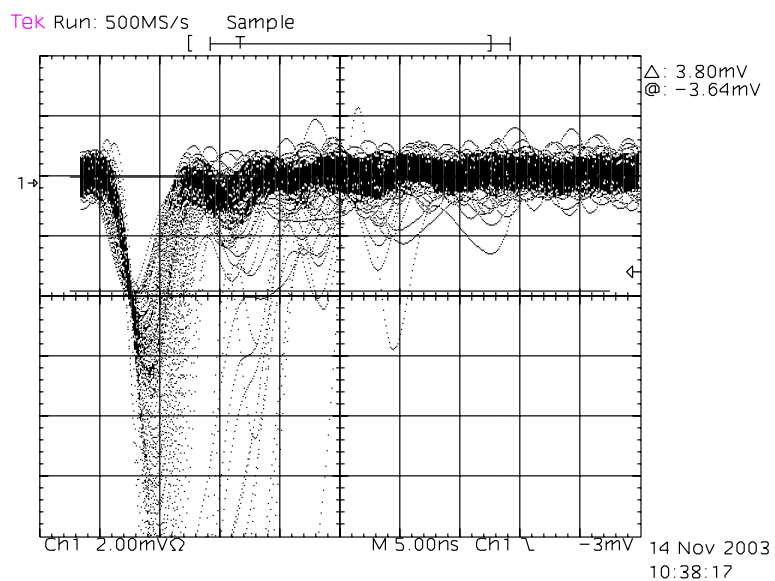


Figure 4: Halo 3, signal triggered on discriminated signal

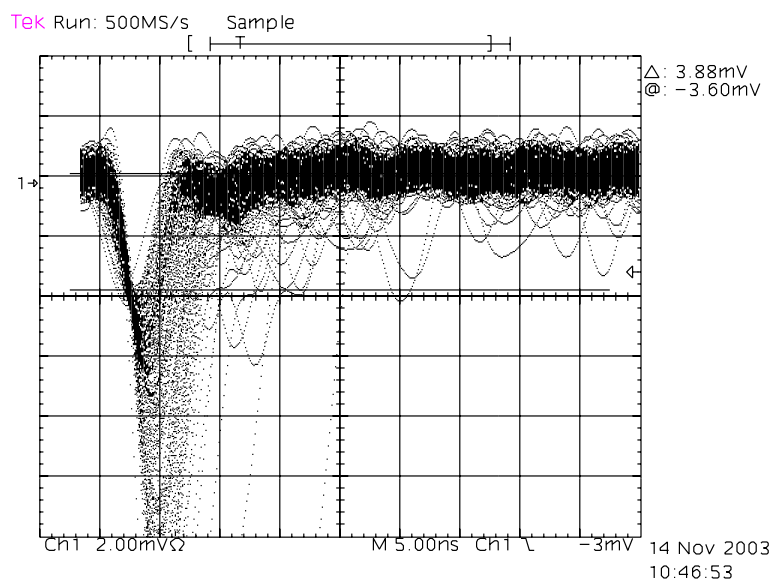
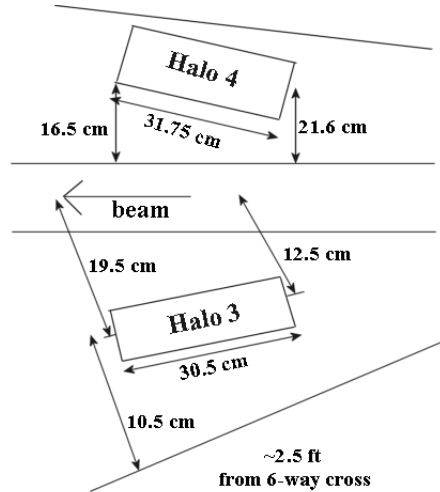


Figure 5: Halo 4, signal triggered on discriminated signal



(image not to scale)

Figure 6: Placement of Detectors Along Beam Line

Once the halo monitors were installed in the hall and the experiment started to run, the data had to be analyzed. There is a huge volume of information is being collected every moment the beam is on, so the relevant numbers have to be selected out of storage for processing. To do this, C++ programs including commands in ROOT[10] and MySQL[11] were needed. C++ provided the framework for the program which then was sent running errands in the other languages to fetch data from the database. The database would then politely return the requested information, and the program could then analyze it and graph the results. [12] is an excellent resource for C (of which C++ is an extension), and proved very helpful. A sample of part of a program written to create graphs of halo rate versus beam current is provided in the appendix.

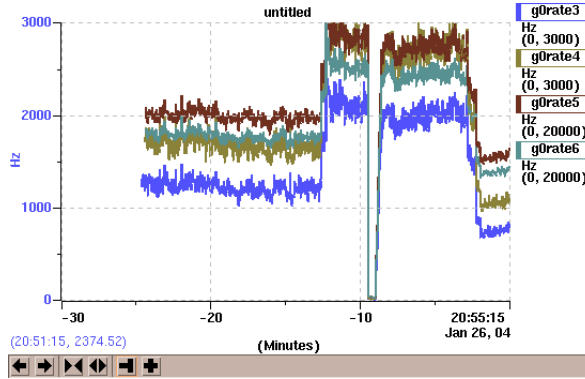


Figure 7: Suspicious Halo Monitor Changes

## 0.4 Analysis and Interpretation of Results

While the experiment is running, the halo monitors give a window into the beam quality. If the halo rates were to suddenly increase, as shown in *Figure 7*, the run leader would be wise to stop the run and try to correct whatever is causing the large halo.

In the case of *Figure 7*, the halo rates actually increased because of changes made to part of the experimental set-up, which were then changed back to their original settings, bringing the rates back down to reasonable levels. However, the sort of change shown could be typical of, though probably much larger in size than, an increase in rates that would arise from mis-steering of the beam.

Looking at the average halo rate over many runs can be useful as well. In particular, the ratios between different halo monitors can illuminate how well they respond to different beam situations. The tables below list the status of the halo target during runs through January and March; *Figures 8- 11* are plots of average halo rate ratios for these runs. Halo monitors 3 and 4, and 5 and 6, are more closely related pairs since each pair has similar high voltage settings and are in mirror positions along the beamline.

### January Runs

Runs 18992 - 19049: 11mm target in  
Runs 19050 - 19111: no halo target  
Runs 19112 - 19161: 11mm target in  
Runs 19162 - 19176: no halo target  
Runs 19177 - 19263: 11mm target in  
Runs 19264 - 19267: 6mm target in  
Runs 19268 - 19286: 11mm target in  
Runs 19287 - 19299: 6mm target in  
Runs 19300 - 19340: 11mm target in  
Runs 19340 - 19342: no halo target  
Runs 19343 - 19417: 11mm target in  
Runs 19418 - 19571: 6mm target in

### March Runs

Runs 20452 - 20456: 6mm target in  
Run 20457: no halo target, coil pulsing  
Runs 20458 - 20462: 6mm target in  
Run 20463: no halo target, coil pulsing  
Runs 20464 - 20490: 6mm target in  
Runs 20492 - 20503: 6mm target in  
Run 20504: 6mm target, no beam  
Runs 20505 - 20512: 6mm target in  
Runs 20513 - 20514: 6mm target in  
Runs 20516 - 20535: 6mm target in  
Runs 20537 - 20562: 6mm target in  
Run 20618: 6mm target in  
Runs 20619 - 20525: 11mm target in  
Run 20626: 6mm target in  
Run 20627: 6mm target in, coil pulsing  
Run 20628: no halo target, coil pulsing  
Runs 20629 - 20634: 6mm target in  
Runs 20656 - 20658: 6mm target in  
Runs 20672 - 20677: 6mm target in  
Runs 20678 - 20679: 6mm target in, no beam  
Runs 20680 - 20778: 6mm target in

It is perhaps more interesting to focus on the related monitors, since the ratio between the two appears to be more sensitive to beam conditions. From these plots times of "good beam" and "bad beam" can be observed. From all of the ratios, however, it is apparent that the monitors scale together quite well and react in predicted ways to changes of the halo target.

To relate the rates from the halo monitors to the beam current (measured by two beam current

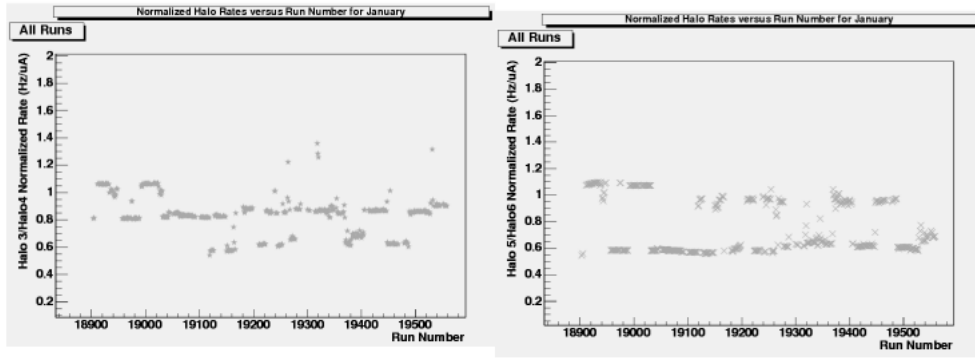


Figure 8: January Ratios of Related Monitors

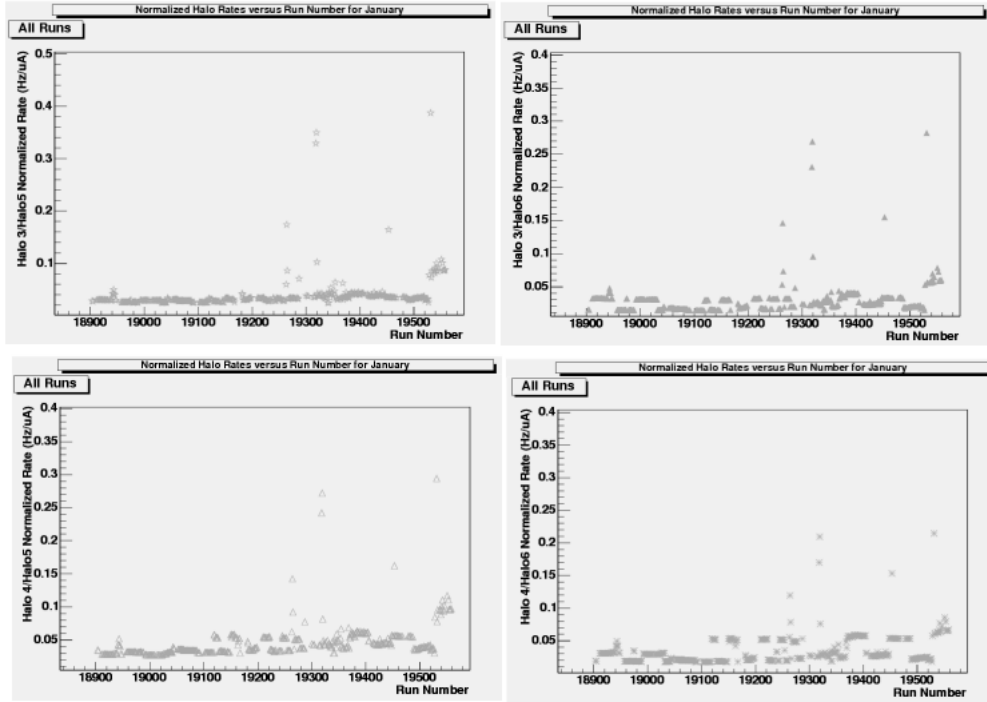


Figure 9: January Ratios of Less Related Monitors

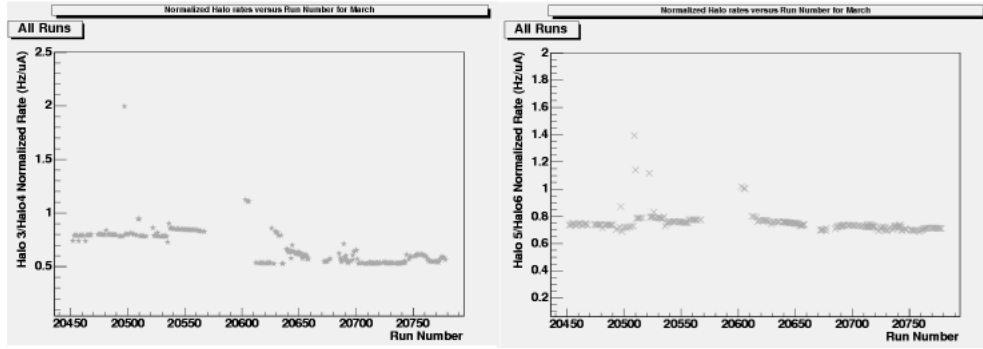


Figure 10: March Ratios of Related Monitors

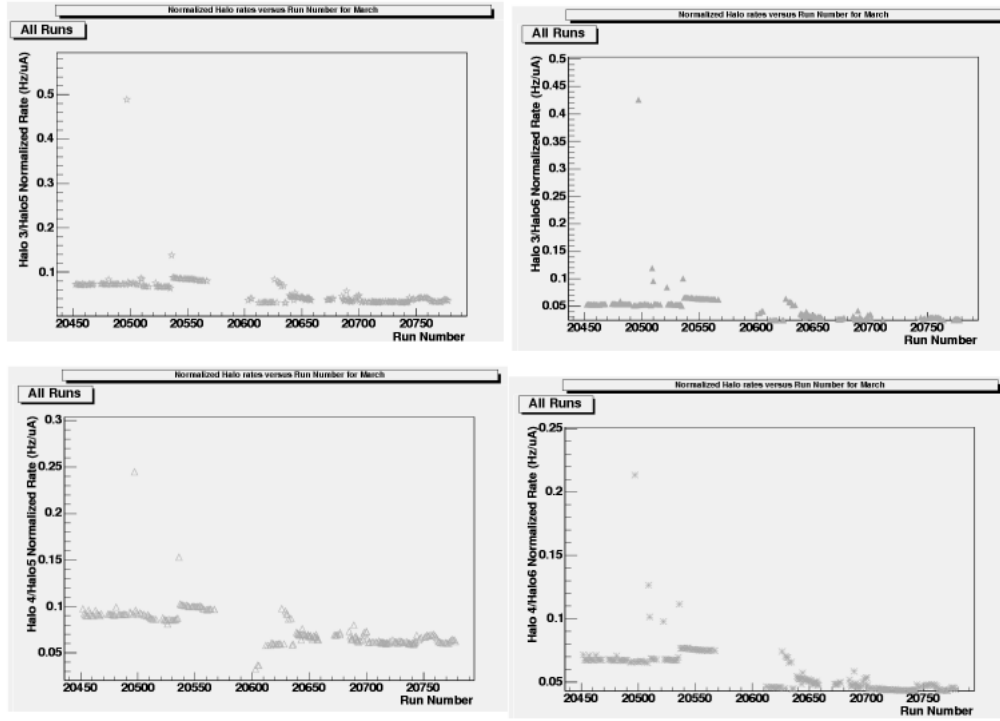


Figure 11: March Ratios of Less Related Monitors



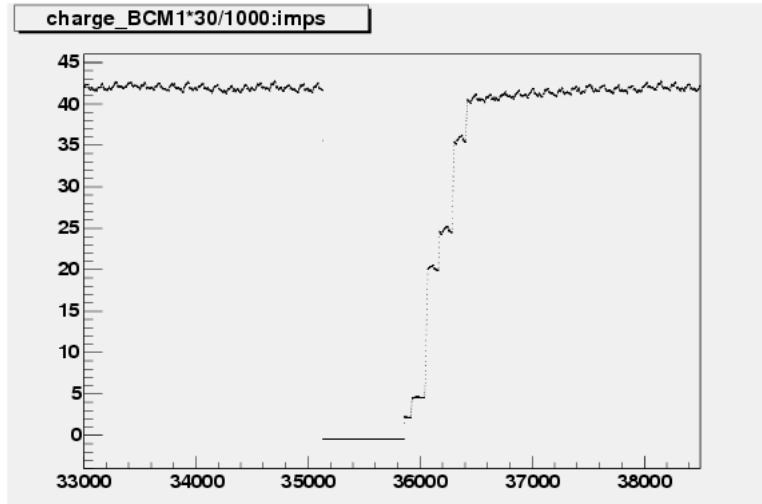


Figure 12: Beam Trip in Run 21168

monitors, BCM1 and BCM2), it's useful to look at times where the beam current is changing in an understood manner. One such time is when the beam is coming back after a beam trip. When the beam trips off, the beam is brought back in small steps until it reaches  $40 \mu\text{A}$ , as visible in *Figure 12*, from Run 21168. BCM1 is multiplied by 30 to account for the 30 Hz cycling between right- and left-handed helicity electrons, and divided by 1000 to change the units from amps to milliamps; imps is a measure of time. *Figure 13* shows a closer view of the first three steps of beam coming back. *Figure 14* is the same graph, only plotting Halo 3 rather than BCM1. It's evident that there is not enough data in *Figure 14* to be statistically significant, or even sensible, so looking into beam trips is not a worthwhile source of halo data.

Since the steps during the ramping up of the beam after a beam trip are too small to yield any useful information, we look instead to BCM calibration runs. In these, the current is stepped up from  $5 \mu\text{A}$  to  $40 \mu\text{A}$  in  $5 \mu\text{A}$  increments. Data from Halos 3-6 from Runs 20481 and 20009, BCM calibration runs with the 6mm halo target in place, was extracted manually from ROOT and then

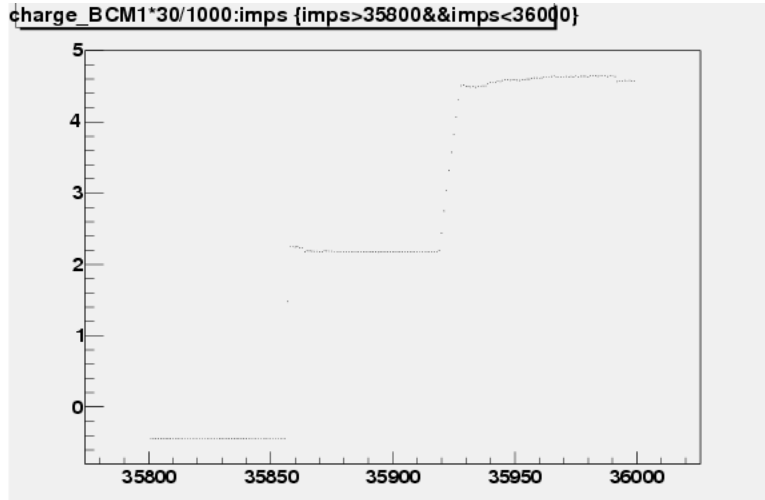


Figure 13: First Three Steps in Beam Current After Beam Trip in Run 21168

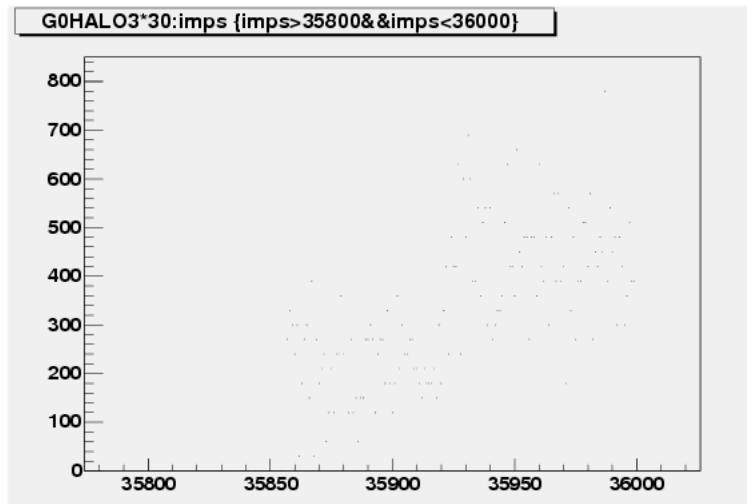


Figure 14: Halo 3 During the First Three Steps in Beam Current After Beam Trip in Run 21168

explicitly filled into arrays in a C++ program that then had ROOT plot the results. The raw rates are shown in *Figure 15*. The raw rates were then normalized against Run 20352, when the halo target was out of the beam: these normalized rates are shown in *Figure 16*.

From these plots, it is evident that the halo monitors scale together. Each of the runs is fairly linear, so there was no increase in halo during the run. The first point from Run 20481 seems abnormally high; this is most likely attributable to beam steering. It is fairly clear, as shown in *Figures 17* and *18*, that the beam position, in both the x- and y-directions, was off by about a factor of two. It was most likely this measurable difference that caused an increased halo rate, because the mis-steered beam would scrape against the halo target walls and create a shower.

## 0.5 Conclusions

The raw data this analysis is based on was expected to be in hand beginning in October of 2003. Hurricane Isabel, however, robbed the area of its electricity for several days, which forced JLab's cryo system to be down for the first time. This introduced over a month's worth of work at the lab bringing everything back online, and the  $G^0$  experiment started much later than originally planned. Thus I was unable to start analysis until the spring semester began. Despite this considerable setback, some valuable information has been gleaned. The halo monitors are a very valuable aspect of the beam monitoring system in place while data is being taken on the experiment.

During the fall semester, I worked with Sarah Phillips to characterize and install halo monitors 3 and 4. Halos 3 and 4 performed like healthy PMTs in the lab, responding at appropriate voltage settings with signals with short rise times. We mounted them in the Hall C on either side of the beamline, making them a part of the halo monitor array positioned for continuous monitoring of the electron beam.

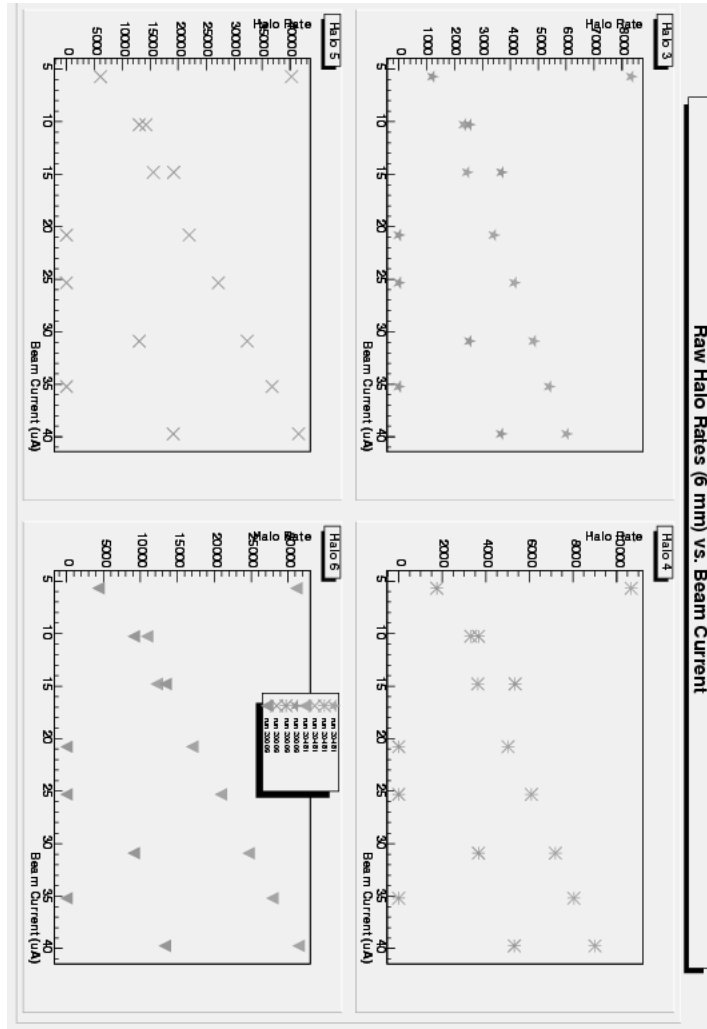


Figure 15: Raw Halo Rates for Beam Current Monitor Calibration Runs 20009 and 20481

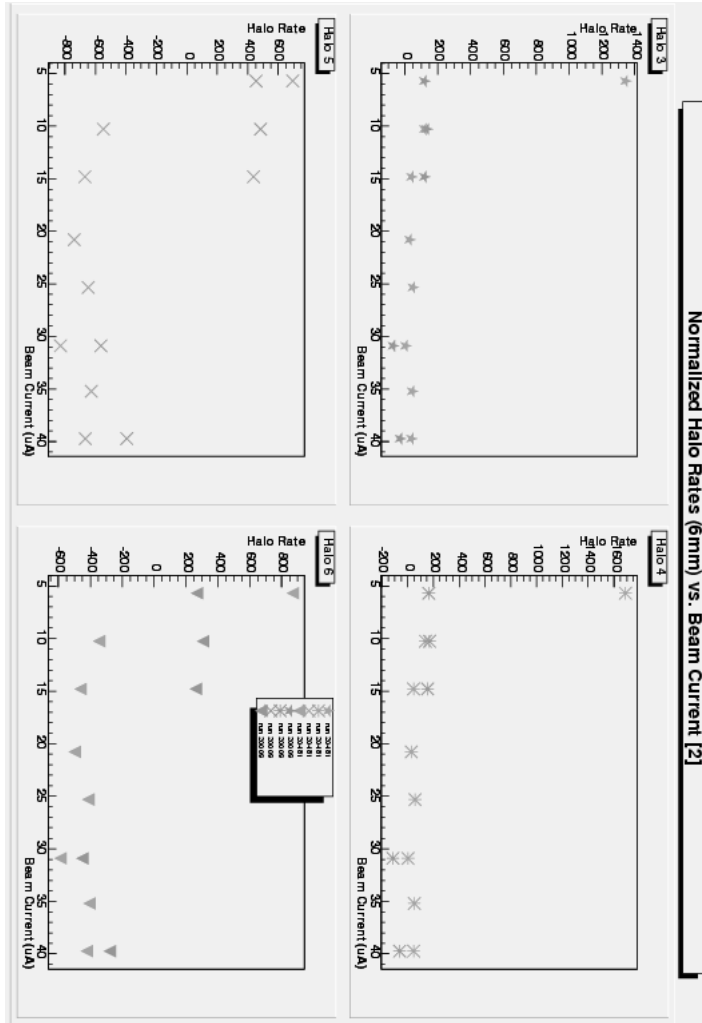


Figure 16: Normalized Halo Rates for Beam Current Monitor Calibration Runs 20009 and 20481

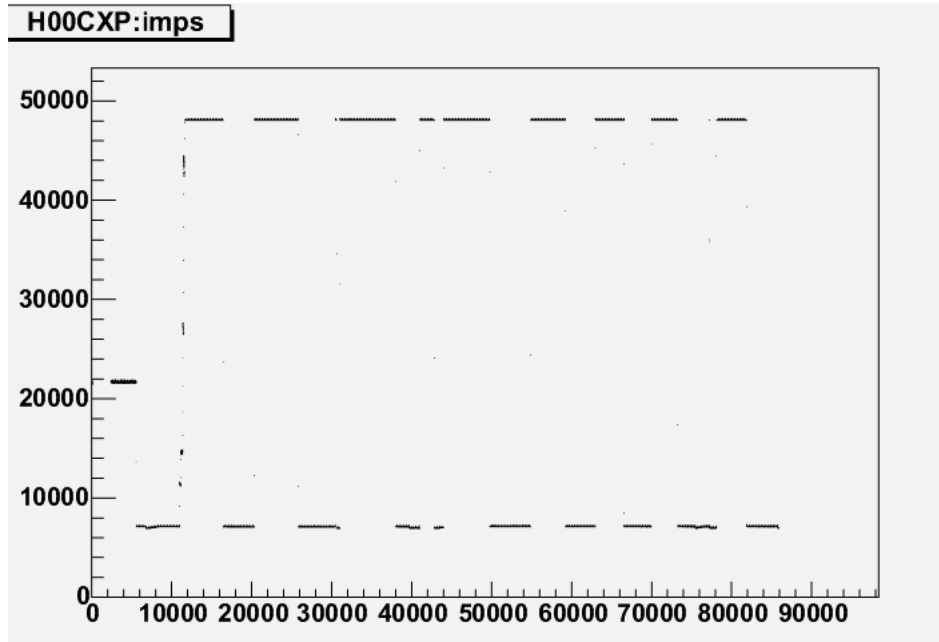


Figure 17: Run 20481, X-Position of the Beam

Once the experiment began production runs, these halo monitors characterized the beam in real-time, which allowed the run leader to stop a run and correct beam steering if the halo rates were outside the acceptable range (beam steering is often the source of an abnormally high halo rate, as the beam scraping the sides of the halo target creates a particle shower). Data from the halo monitors also provides a way to analyze the size of the beam halo after the run has been taken, so that an idea of the overall quality of the electron beam can be formed. As explained earlier, the different monitors scale together well, and the relationship between halo rates and beam charge is well-established.

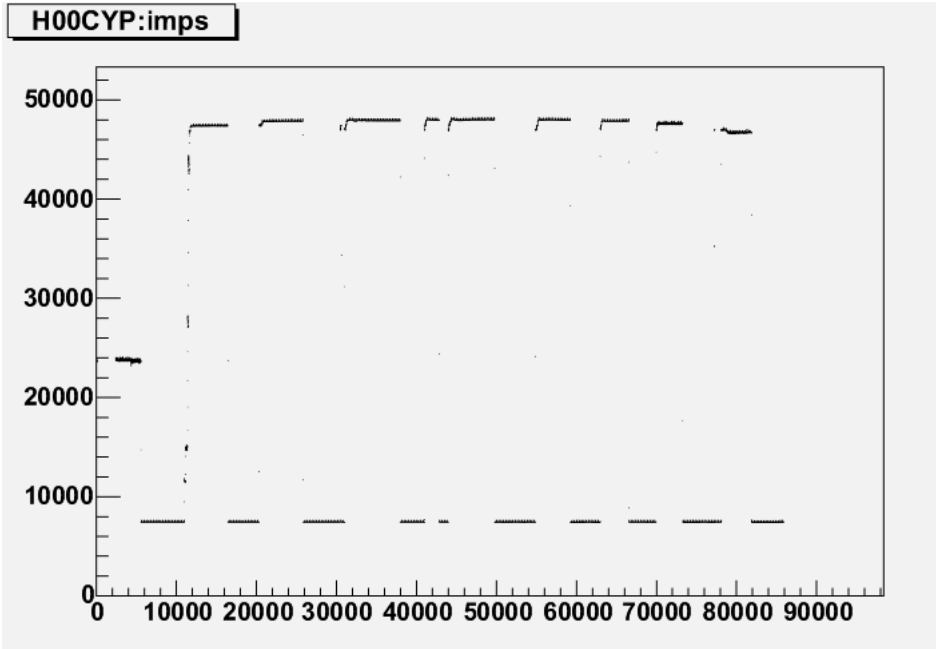


Figure 18: Run 20481, Y-Position of the Beam

# Bibliography

- [1] G0 Home Page. <http://www.npl.uiuc.edu/exp/G0>
- [2] I.S. Hughes, *Elementary Particles*, Cambridge University Press, Cambridge, (1991).
- [3] D.S. Armstrong, *Strange Quark Content of the Nucleon*, Proc. 18th Winter Workshop on Nuclear Dynamics, (2002).
- [4] D.H. Beck and B.R. Holstein, *Nucleon Structure and Parity-Violating Electron Scattering*, International Journal of Modern Physics E, World Scientific Publishing Company, (2001).
- [5] E.J. Beise, *Parity Violation with Electrons and Hadrons*, arXiv:nucl-ex/309008, (2003) [Invited talk at the 17th International IUPAP Conference on Few-Body Problems in Physics].
- [6] P. Adderly, M. Baylac, J. Clark, T. Day, J. Grames, J. Hansknecht, M. Poelker, M. Stutzman, *Jefferson Lab Polarized Source*, Mainz Parity Workshop Proceedings (2002).
- [7] D. Beck, “ $G^0$ ”: *Measurement of the Flavor Singlet Form Factors of the Proton* [JLab experiment E91017 abstract].
- [8] G0 at IPNO-RDD. <http://ipnweb.in2p3.fr/rdd/G0/>
- [9] Sarah K. Phillips, *Beam Halo in the First  $G^0$  Engineering Run*, Williamsburg, VA (2003) (unpublished) [draft].



[10] The ROOT System Home Page. <http://root.cern.ch>

[11] MySQL: The World's Most Popular Open Source Database. <http://www.mysql.com>

[12] Brian W. Kerningham and Dennis M. Ritchie, *The C Programming Language*, Prentice-Hall Inc, New Jersey (1978).

## .1 Sample Code

Below are sections of a program that creates plots from points extracted manually from the database.

Comments are prefaced by `//`.

```
Int_t graph1(Int_t NumOfFiles,Float_t Beam_Current[],Float_t Beam_Currentb[],Float_t x1[],Float_t
x1b[],Float_t x2[],Float_t x2b[],Float_t x3[],Float_t x3b[],Float_t x4[],Float_t x4b[],char *t);
int main(int argc, char** argv)
{
TApplication theApp("App", &argc, argv);
gStyle->SetOptFit(0111);
//ROOT commands

char t[50];
Int_t NumOfFiles=8;
Float_t x1[NumOfFiles];
//etc. through x4
Float_t x1b[NumOfFiles];
//etc. through x4b
//string, number, and arrays to be filled with data passed to graph1 for each graph created
```

```
Float_t Beam_Current[]={5.688,10.27,14.81,20.78,25.32,30.89,35.21,39.72};
```

```
//values 20 and above are BCM1, below 20 are BCM2
```

```
Float_t Halo3raw[]={8324,2331,2447,3399,4137,4826,5389,6015};
```

```
Float_t Halo4raw[]={10660,3305,3625,5010,6090,7194,8030,9002};
```

```
Float_t Halo5raw[]={40250,14190,15530,21970,27140,32300,36780,41500};
```

```
Float_t Halo6raw[]={31110,10940,12230,17020,20900,24680,27870,31420};
```

```
Float_t Beam_Currentb[]={4.969,10.38,15.1,31.04,44.91};
```

```
Float_t Halo3rawb[]={1197,2521,3683,2521,3661};
```

```
Float_t Halo4rawb[]={1741,3652,5342,3651,5311};
```

```
Float_t Halo5rawb[]={6077,13060,19200,13050,19080};
```

```
Float_t Halo6rawb[]={4291,9109,13420,9109,13340};
```

```
Float_t Beam_Currentnohalo[]={5.187,10.16,14.94,20.32,25.06,29.77,36.09,39.62};
```

```
Float_t Halo3nohalo[]={631.8,1115,1869,2750,2893,4572,3926,4452};
```

```
Float_t Halo4nohalo[]={968.8,1869,2960,4300,4625,6883,6351,7141};
```

```
Float_t Halo5nohalo[]={3994,7885,12480,18360,20340,29370,28210,32460};
```

```
Float_t Halo6nohalo[]={3086,5815,9372,13480,14440,22150,20180,22780};
```

```
Float_t Halo3[NumOfFiles];
```

```
//etc. through Halo6b
```

```

Float_t Halo3n[NumOfFiles];

//etc. through Halo6bn

for (int a=0; a<NumOfFiles; a++) {
Halo3n[a]=((Halo3raw[a]/Beam_Current[a])-(Halo3nohalo[a]/Beam_Currentnohalo[a]));
//etc. through Halo6n
}

for (int b=0; b<NumOfFiles; b++) {
Halo3bn[b]=((Halo3rawb[b]/Beam_Currentb[b])-(Halo3nohalo[b]/Beam_Currentnohalo[b]));
//etc. through Halo6bn
}

//the above for loops create arrays of the normalized halo rate

for(int i=0;i<NumOfFiles;i++) {
x1[i]=Halo3n[i];
//etc through x4b[i]=Halo6bn[i];
}

char title3[50] = "Normalized Halo Rates (6mm) vs. Beam Current [2]\0";
t = title3;

```

```

TCanvas* MyCanvas3 = new TCanvas("MyCanvas3", "graph", 1);
graph1(NumOfFiles,Beam_Current,Beam_Currentb,x1,x1b,x2,x2b,x3,x3b,x4,x4b,t);
TString filename3;
filename3 = "/work/hallc/gzero/acslau/g0scratch/scripts/March16/normrates32.ps";
MyCanvas3->SaveAs(filename3);

theApp.Run();

return(0);
}

Int_t graph1(Int_t NumOfFiles,Float_t Beam_Current[],Float_t Beam_Currentb[],Float_t x1[],Float_t
x1b[],Float_t x2[],Float_t x2b[],Float_t x3[],Float_t x3b[],Float_t x4[],Float_t x4b[],char *t)
{
//this function tells ROOT how to format the graph being created

TPaveLabel* title = new TPaveLabel(0.1,0.96,0.9,0.99,t);
title->Draw();

TDateTime* now;
now = new TDateTime();

```

```

TPaveLabel* date = new TPaveLabel(0.7,0.01,0.9,0.03,now->AsString());
date->Draw();

TPad* graphPad1 = new TPad("Graphs","Graphs",0.01,0.05,0.95,0.95);
graphPad1->Draw();
graphPad1->cd();
graphPad1->Divide(2,2);
graphPad1->cd(1);

TGraph* gr1 = new TGraph(NumOfFiles,Beam_Current,x1);
TGraph* gr2 = new TGraph(NumOfFiles,Beam_Current,x2);
//etc. through gr4b

gr1->SetMarkerColor(8);
gr1->SetMarkerStyle(29);
//etc through gr4b

TMultiGraph* mg1 = new TMultiGraph();
mg1->SetTitle("Halo 3");
mg1->Add(gr1);
mg1->Draw("AP");
mg1->Add(gr1b);
mg1->Draw("P");

```

```

mg1->GetXaxis()->SetTitle("Beam Current (uA)");
mg1->GetYaxis()->SetTitle("Halo Rate");
mg1->Draw("AP");

//TMultiGraph* mg2, mg3, mg4 similarly constructed, substituting for Halo number and gr number

TLegend *leg1;

leg1 = new TLegend(0.45,0.85,0.55,0.99);
leg1->AddEntry(gr1,"run 20481", "p");
leg1->AddEntry(gr2,"run 20481", "p");
leg1->AddEntry(gr3,"run 20481", "p");
leg1->AddEntry(gr4,"run 20481", "p");
leg1->AddEntry(gr1b, "run 20009", "p");
leg1->AddEntry(gr2b, "run 20009", "p");
leg1->AddEntry(gr3b, "run 20009", "p");
leg1->AddEntry(gr4b, "run 20009", "p");
leg1->Draw();

}

```